Available online at www.sciencedirect.com

ScienceDirect

journal homepage: www.elsevier.com/locate/he

Aligned polyaniline nanorods in situ grown on gas diffusion layer and their application in polymer electrolyte membrane fuel cells

Xudong Fu [a,b], Suli Wang [a], Zhangxun Xia [a], Yinhua Li [a], Luhua Jiang [a], Gongquan Sun [a,*]

[a] Division of Fuel Cell & Battery, Dalian National Laboratory for Clean Energy, Dalian Institute of Chemical Physics, Chinese Academy of Sciences, Dalian 116023, China

[b] University of Chinese Academy of Sciences, Beijing 100039, China

ARTICLE INFO

Article history:
Received 8 October 2015
Received in revised form
14 December 2015
Accepted 29 December 2015
Available online 21 January 2016

Keywords:
Polyaniline nanorod
Ordered catalyst layer
In situ polymerization
Polymer electrolyte membrane fuel cell
Oxygen transport

ABSTRACT

Catalyst layers (CLs) with spatially ordered structure can improve mass transport of reactants/products, which is essential for the high performance of polymer electrolyte membrane fuel cells (PEMFCs). In this study, aligned polyaniline (PANI) nanorods grown on gas diffusion layers by in situ polymerization are used as supports for platinum to fabricate ordered CLs. The length and diameter of the PANI nanorods can be controlled by optimizing the reaction temperatures or the aniline concentrations during the in situ polymerization process. With the optimized aligned PANI nanorods as supports of cathode, the mass specific power density of the PEMFC reaches 2.5 kW g_{Pt}^{-1}, which is 21% higher than that of the conventional PEMFC without PANI. This improvement can be attributed to the reduced oxygen transport resistance revealed by oxygen gain and electrochemical impedance spectroscopy.

Introduction

Polymer electrolyte membrane fuel cells (PEMFCs) have gained numerous attentions because of their high energy density, low temperature operation and environmental benefits [1–4]. However, the large amount of Pt used for catalyzing the oxygen reduction reaction at the cathode has hampered the widespread application of PEMFCs. The reduction of the Pt usage is considered to be a critical challenge for widely commercialization of PEMFCs. Unfortunately, reducing Pt loading generally could induce the cell performance loss, partially due to the increased oxygen transport resistance [5]. Minimizing the oxygen transport resistance in the cathode is one of the effective solutions to enhance the cell performance for low Pt loading membrane electrode assembly (MEA). It is generally accepted that the oxygen transport from the flow field to the catalyst layer (CL) in the cathode of a PEMFC follows two diffusion processes: molecular diffusion dominates in the carbon paper and Knudsen diffusion dominates in the microporous layer (MPL) and the CL. The effective diffusion coefficient of molecular diffusion is three orders of magnitude

* Corresponding author. Tel./fax: +86 411 84379063.
E-mail address: gqsun@dicp.ac.cn (G. Sun).

http://dx.doi.org/10.1016/j.ijhydene.2015.12.193

higher than that of Knudsen diffusion. Hence, the oxygen transport resistance of the cathode is mainly resulted from the diffusion of oxygen across the MPL and CL. Many efforts have been carried out to improve the oxygen transport in cathodes of PEMFCs. Yang and Middelman found that oxygen mass transport could be improved with networked MPL [6,7] and ordered CL [8], respectively. Inspired by the research work related to ordered CL of Middelman, diverse types of spatially ordered CLs were fabricated, which were based on nanostructured thin films [9], columnar carbon layer [10], vertically aligned carbon nanotubes or nanofibers (VACNT/VACNF) arrays [11,12] and vertically aligned metal oxides [13] et al., yet these ordered CLs commonly needed complex preparation process such as plasma sputter deposition [9,10], chemical vapor deposition [11,12] and glancing angle deposition [13].

The low cost of polyaniline (PANI), combined with its high conductivity in partially oxidized state [14], high chemical stability in acid medium [15], good thermal conductivity [16,17], as well as its facile to be constructed in ordered nanostructure, e.g. nanorod array, nanotube array etc, make it an appealing electrocatalyst support in PEMFCs. It is reported that aligned PANI nanorods can be assembled by electrochemical method [18] and dilute polymerization method [19]. The electrochemical method is limited to a small scale, because the current distribution may be uneven in different positions of the substrate, leading to an undesired structure of the PANI nanorods. Compared with electrochemical method, dilute polymerization method is much more facile for the synthesis of large area aligned PANI nanorods. But the method is limited to flat substrates, such as polytetrafluoroethylene (PTFE), polystyrene (PS) and glass, and there are few reports about the aligned PANI nanorods obtained on porous substrates up to now. In this article, for the first time, we report that aligned PANI nanorods are grown on porous gas diffusion layer (GDL) by in situ polymerization. The length and diameter of the PANI nanorods can be controlled by tuning the reaction temperatures or the aniline concentrations during the polymerization. With the optimized aligned PANI nanorods as supports of cathode, performance of the PEMFC single cell is improved, and the mechanism for performance improvement is investigated by oxygen gain and electrochemical impedance spectroscopy (EIS).

Experimental

Materials

All chemicals were used as received without further purification. Aniline and $(NH_4)_2S_2O_4$ (APS) were purchased from Tianjin Damao Reagent. $HClO_4$ was purchased from Tianjin Zhengcheng Reagent. Pt black and 60 wt.% Pt/C were purchased from Johnson Matthey Co., Ltd. Nafion® solution (5 wt.%) and Nafion® 212 membrane were purchased from DuPont Corporation. Carbon paper (TGP-H-060) with a porosity of 78% was purchased from Toray, Japan [17]. All aqueous solutions were prepared with ultrapure water from a Unique-R20 water system.

Preparation of aligned PANI nanorods on GDLs

The GDL was made up of hydrophobic carbon paper and MPL. The hydrophobic carbon paper was prepared by spraying the 1 wt.% PTFE solution onto the carbon paper, dried in air, and sintered at 340 °C. The amount of PTFE in hydrophobic carbon paper was approximately 10 wt.%. Then, the carbon powder (Vulcan XC-72, Cabot Corp.), 60 wt.% PTFE, and ethanol were ultrasonically mixed with a weight ratio 3:2 of carbon to solid PTFE content. The viscous mixture was coated onto hydrophobic carbon paper and then heated at 340 °C for 1 h. The carbon powder of MPL was controlled at 0.5 mg cm^{-2}.

Aligned PANI nanorods were synthesized by a modified dilute polymerization method as previously reported [19]. In a typical procedure, aniline monomer or oxidant (APS) was added into 100 ml $HClO_4$ solution (aqueous, 1 mol L^{-1}) and stirred for 5 min to form a uniform solution, respectively, where the molar ratio of aniline to APS was 1.5. The two solutions were kept in a certain temperature. The polymerization was performed by rapidly adding the oxidant solution to the aniline solution and a piece of GDL (4 × 4 cm^2) was immersed into the mixed solution, where the MPL of the GDL faced to the solution while the other side was sealed. Then, the mixture remained still for 24 h. Finally, the GDL was taken out and washed with ultrapure water. The samples polymerized at −5 °C, 0 °C, 10 °C or 25 °C with an aniline concentration of 10 mmol L^{-1} were denoted as PANI-T-5, PANI-T0, PANI-T10 or PANI-T25, respectively. To investigate the effect of aniline monomer concentration on the morphology of PANI, the concentrations of aniline monomer were kept at 5 mmol L^{-1}, 8 mmol L^{-1}, 10 mmol L^{-1}, 12 mmol L^{-1}, 15 mmol L^{-1} and 20 mmol L^{-1} while the temperature was kept at 0 °C. The PANI in the solution was filtrated and washed several times with ultrapure water, and finally dried at 60 °C to obtain green powder. The corresponding samples were denoted as PANI-C5, PANI-C8, PANI-C10, PANI-C12, PANI-C15 or PANI-C20, respectively.

Characterizations of the aligned PANI nanorods

Characterizations of the aligned PANI nanorods on GDLs were investigated by Scanning Electron Microscope (SEM, JSM-7800F, JEOL), Attenuation Total Reflection Fourier Transformed Infrared Spectroscopy (ATR-FTIR, Nicolet 6700, Thermo Fisher). The in-plane conductivity of the PANI was characterized by four point probe method (SZ-82, Suzhou Telecommunication). Considering the conductivity of the PANI nanorods on the GDLs was the same as PANI powder obtained from the solution. The detailed measure process was as follows: First, the PANI powder was pressed to a disk. Then three different points of every disk were tested and the mean value was taken.

Fabrication of MEA

The GDLs with aligned PANI nanorods were cut into 2 × 2 cm^2. The cathodes were obtained by spraying catalyst ink composed of commercial Pt black and Nafion® ionomer onto the GDLs with PANI nanorods. For comparison, the GDL without PANI was used to prepare cathode following the

similar process. The Pt loading on the cathodes was about 0.15 mg cm^{-2}. Anodes were prepared by spraying catalyst ink composed of commercial 60 wt.% Pt/C and Nafion® ionomer onto the anode GDLs with Pt loading of about 0.25 mg cm^{-2}. Since the effect of aligned PANI nanorods on the performance of cathodes was studied in this work, the Pt loading of the anode was higher than that of cathode to eliminate the effect of anode. Nafion® 212 membrane sandwiched between the anode and the cathode was pressed at 120 °C and 50 kg cm^{-2} for 1 min. The PANI nanorods were not deformed when the mechanical stress is lower than 280 kg cm^{-2} [19], so the PANI nanorods could maintain in the hot press process.

PEMFC single cell performance tests

The performances and durability of PEMFCs were evaluated at 80 °C using a single cell with serpentine flow channels via a Fuel Cell Test Station (Green Light Innovation, G20 HT). The anode side was fed with hydrogen at a flow rate of 200 mL min^{-1}, and the cathode side was fed with oxygen at a flow rate of 400 mL min^{-1} at a total outlet pressure of 150 kPa on both sides. The hydrogen and oxygen were externally humidified at dew point temperature of 80 °C and 70 °C, respectively. The PEMFCs were activated at 0.7 V until two polarization curves of every PEMFC were coincidental. Then the anode side was fed with hydrogen and served as the reference and counter electrodes. The cathode side was fed with nitrogen and served as the working electrode. The flow rate, outlet pressure and the gas humidification temperatures were same with the polarization curves test. The cyclic voltammetry (CV) measurements were performed using an electrochemical workstation (SI1287, Solartron Co.) in the range of 0.6–1.2 V for 5000 cycles. The polarization curves of the PEMFCs were evaluated after 0, 1000, 3000 and 5000 cycles.

EIS was carried out at the applied current of 1000 mA cm^{-2} via an electrochemical workstation (SI1287 and SI1260, Solartron Co.). The alternating current (AC) potential frequency range was 10 kHz–0.1 Hz with an amplitude of 10 mV. Before each EIS measurement, the single cell was stabilized at the applied current for 20 min. During the EIS test, the operating conditions, including the cell temperature and gas flowing rates, were all kept the same as that in the polarization measurements. The oxygen gain of the PEMFC was the difference of the cell voltages at the same current density when the cathode was fed with oxygen or air.

Results and discussions

Controllable synthesis of the aligned PANI nanorods

Polymerization of aniline in its dilute solution has been successfully used for the preparation of PANI nanorods on various flat substrates [19]. In this study, GDL is used as substrate to grow PANI nanorods. To get PANI nanorods on the porous substrate, the polymerization conditions were optimized firstly. Then Pt black catalyst was sprayed on the PANI nanorods to obtain the cathode CL. The fabrication process of MEA is illustrated in Fig. 1. Fig. 2a shows the surface topography of GDL. It could be seen that carbon nanoparticles with

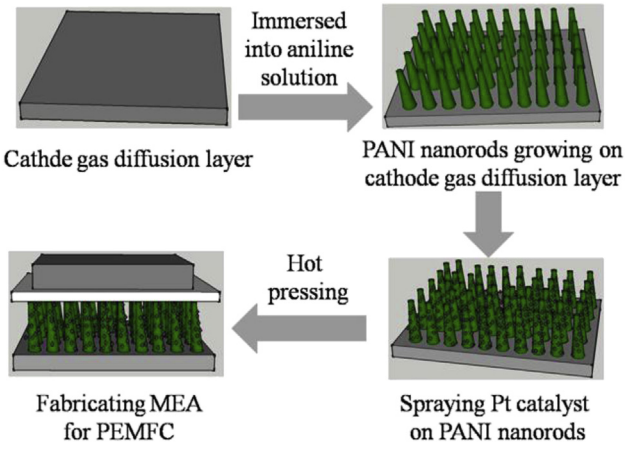

Fig. 1 – Fabrication process of PANI nanorods and MEA for PEMFC.

average diameter of 50–80 nm are randomly accumulated on the surface. Fig. 2b indicates the PANI nanorods are slightly tilted and several PANI nanorods join together into a wider diameter bunch on the GDL.

The influences of polymerization temperatures and aniline concentrations on the PANI morphologies are studied. The temperatures are kept at −5 °C, 0 °C, 10 °C or 25 °C with an aniline concentration of 10 mmol L^{-1}. SEM images and the statistical result of length and diameter of PANI nanorods obtained at different temperatures are shown in Fig. 3. The average diameter of the PANI nanorods obtained at different temperatures is approximate 45 nm. But the average length of PANI nanorods is 135 nm at −5 °C, increasing to 212 nm at 0 °C, and then decreasing to 88 nm at 25 °C. It can be seen that PANI nanorods polymerized at too low (−5 °C, Fig. 3a) or too high (10 °C or 25 °C, Fig. 3c–d) temperature are shorter than those obtained at 0 °C (0 °C, Fig. 3b). So 0 °C is selected in the next part of study.

Fig. 4a–f presents the morphologies of PANI nanorods polymerized at different aniline concentrations. When the concentration of aniline is low (5, 8 mmol L^{-1}, Fig. 4a–b) or high (12, 16, 20 mmol L^{-1}, Fig. 4d–f), the PANI nanorods are shorter than the nanorods obtained at mediate concentration (10 mmol L^{-1}, Fig. 4c). A volcano-like curve is obtained by correlating the average length of PANI nanorods and the aniline concentrations, as shown in Fig. 4g. The average diameter of the PANI nanorods changes unnoticeably with changing aniline concentrations and keeps at about 45 nm. It is interesting to note that the diameter of PANI nanorods obtained at different polymerization temperatures is almost the same to that obtained at different aniline concentrations, which is similar to the size of carbon nanoparticles on the GDL as shown in Fig. 2a.

The influence of aniline concentrations and polymerization temperatures on the PANI morphologies can be explained by the polymerization mechanism. Two possible nucleation sites (bulky solution and carbon nanoparticles in the GDL) compete with each other in the chemical oxidation polymerization process of aniline [20]. When the concentration of aniline monomer is 10 mmol L^{-1} and the temperature is 0 °C,

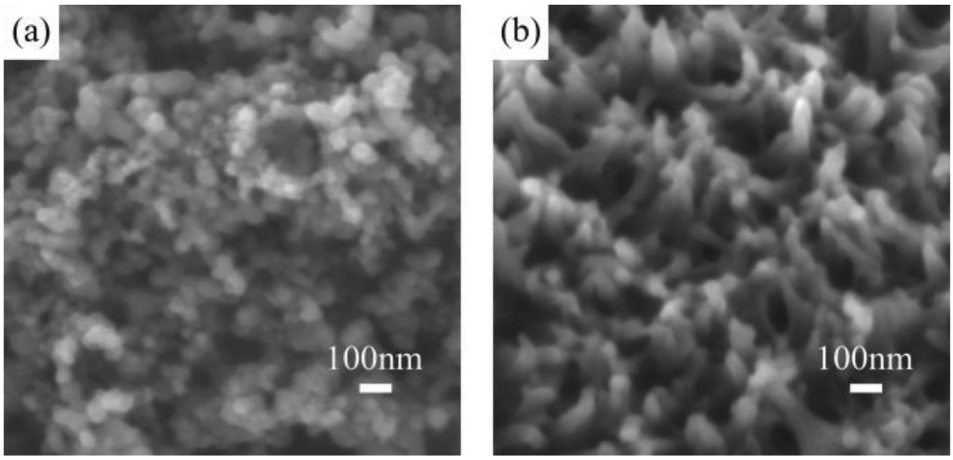

Fig. 2 – SEM images of GDL (a) and PANI-C10 (b).

the rate of polymerization is proper. Then active nucleation sites are generated on the carbon nanoparticles surface at the beginning of the polymerization process by heterogeneous nucleation. These active sites would minimize the interfacial energy barrier between the carbon nanoparticles surface and bulk solution, which is beneficial to the subsequent growth of PANI on the GDL [21]. At the same time, the proper polymerization rate can suppress the homogeneous nucleation in the bulky solution. PANI nanorods will further grow along the initial nuclei, and therefore, long aligned PANI nanorods on GDL are obtained. However, when the temperature is below 0 °C or the concentration of the aniline is below 10 mmol L^{-1}, the amount of aniline diffusing from the bulky solution to the GDL surface is less. Then the PANI nanorods are short. On the contrary, the rate of polymerization is fast. Then homogeneous nucleation in the bulky solution will be dominant after initial nucleation on the carbon nanoparticles surface. Most PANI forms in the bulky solution. So PANI nanorods on the GDL are short, too.

Characterizations of the PANI nanorods

The PANI-C5, PANI-C10 and PANI-C20 are chosen to fabricate PEMFCs, so the three samples are characterized. Fig. 5 shows the ATR-FTIR spectra of the GDL, PANI-C5, PANI-C10 and PANI-C20. For the GDL, the peaks at 1199 cm^{-1} and 1145 cm^{-1} are assigned to anti-symmetric and symmetric stretching vibration of C–F in PTFE, respectively [22]. The other three FTIR spectra are in good agreement with previously reported spectra of PANI [23–25]. The peaks at 1558 cm^{-1} and 1477 cm^{-1} correspond to the stretching deformation of quinoid and benzene rings, respectively, indicating that the obtained PANI is in its conducting emeraldine state, rather than leucoemeraldine or permigraniline state [23]. The 1307 cm^{-1} peak is assigned to the C–N stretching of the secondary aromatic amine and the peak at 1241 cm^{-1} is ascribed to the $C–N^+$ stretching vibration in the polaron structure, indicating that the PANI is in the doped state [24]. In addition, absorption bands at 1142 cm^{-1} and 801 cm^{-1} are originated from the plane-bending vibrations and the out-of-plane bending vibration of C–H of benzene rings during the protonation of $HClO_4$-doped PANI, respectively [25].

The porosity of the porous medium can affect the transport properties. However, the effect of fiber spacing at a constant porosity has been overlooked in the literature. Recently, Sadeghifar et al. showed that the fiber spacing can also be as important as porosity in terms of porous medium transport properties. Such investigations can be useful to the CL structure optimization and further research should be devoted to this new area in the near future [17,26–30]. The porosity of PANI nanorods layer and the density of the PANI nanorods are showed in Table 1. The porosity of the PANI-C10 (91.75%) is larger than that of the PANI-C5 (90.65%) and the PANI-C20 (86.72%). On the contrary, the density of the PANI-C10 (37 μm^{-2}) is lower than that of the PANI-C5 (63 μm^{-2}) and the PANI-C20 (143 μm^{-2}). So the space between the PANI nanorods of PANI-C10 is largest among the three samples, which is benefit for the oxygen transport. The conductivity of PANI-C10 is 10.3 S cm^{-1} as shown in Table 1, which is the highest among the three samples and the same order to that of PANI in previous report [31].

PEMFCs single cell performances

To further investigate the effect of PANI nanorods as the supports on PEMFCs performances, commercial Pt black catalyst was sprayed onto the PANI nanorods to act as the cathodes of PEMFCs. For comparison, a PEMFC without PANI nanorods was also prepared by spraying Pt black catalyst directly onto cathode GDL. Fig. 6 is the polarization curves and the power density curves of the PEMFCs. Apparently, the PEMFC with PANI-C10 exhibits the best performance with a peak power density of 374 mW cm^{-2}, which is 21% higher than that of the PEMFC without PANI nanorods (peak power density of 310 mW cm^{-2}). For the sample PANI-C5, the PEMFC performance drops (peak power density of 326 mW cm^{-2}), while the PEMFC with PANI-C20 shows the lowest performance (peak power density of 299 mW cm^{-2}). The PEMFC with PANI-C10 generates a mass specific power density of 2.5 kW g_{Pt}^{-1} (as the cathode), which is the half of DOE 2015 target. Further

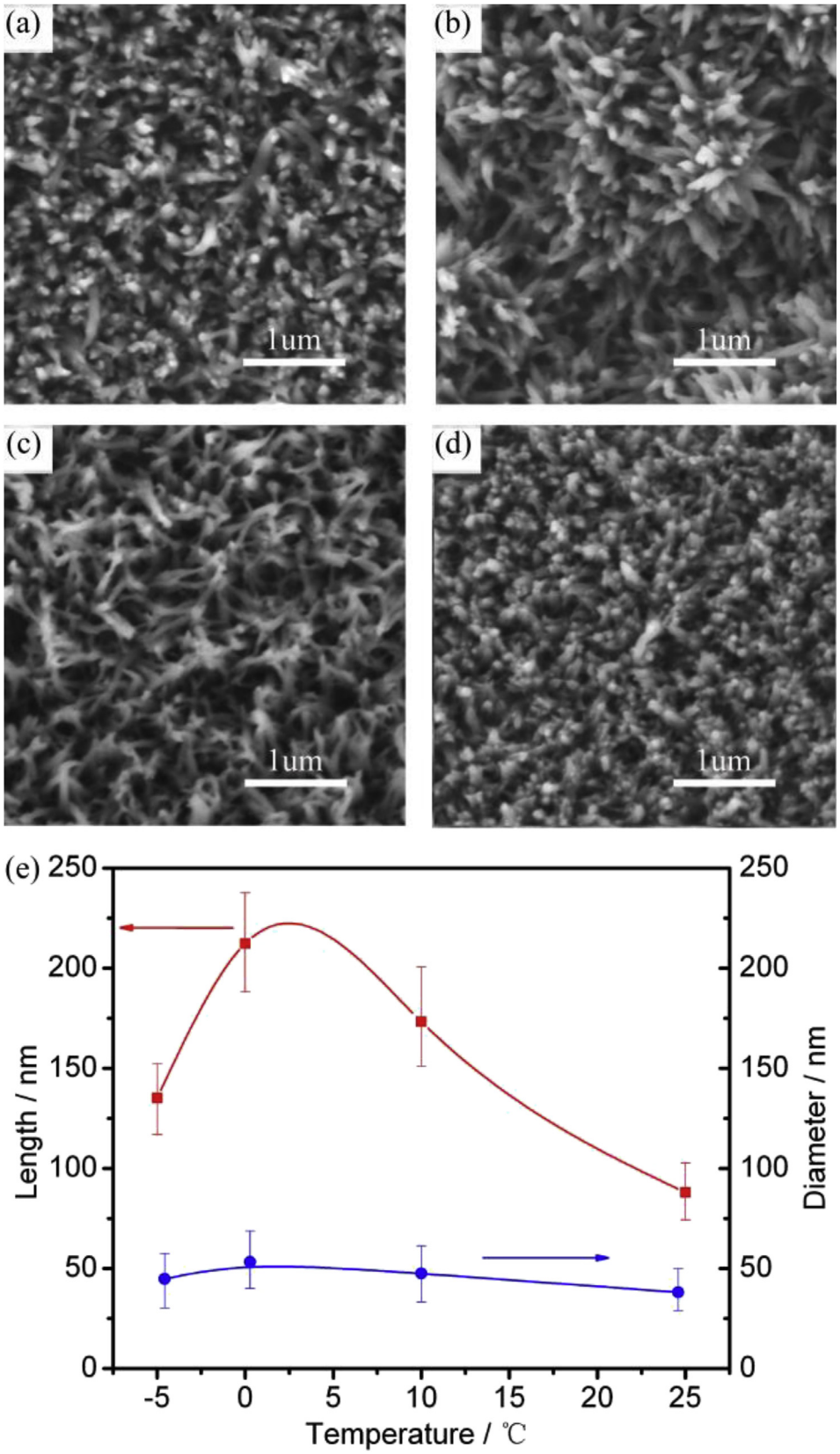

Fig. 3 – SEM images at top view of PANI-T-5 (a), PANI-T0 (b), PANI-T10 (c) and PANI-T25 (d). The variation of the lengths and the diameters of PANI nanorods polymerized at different temperatures (e).

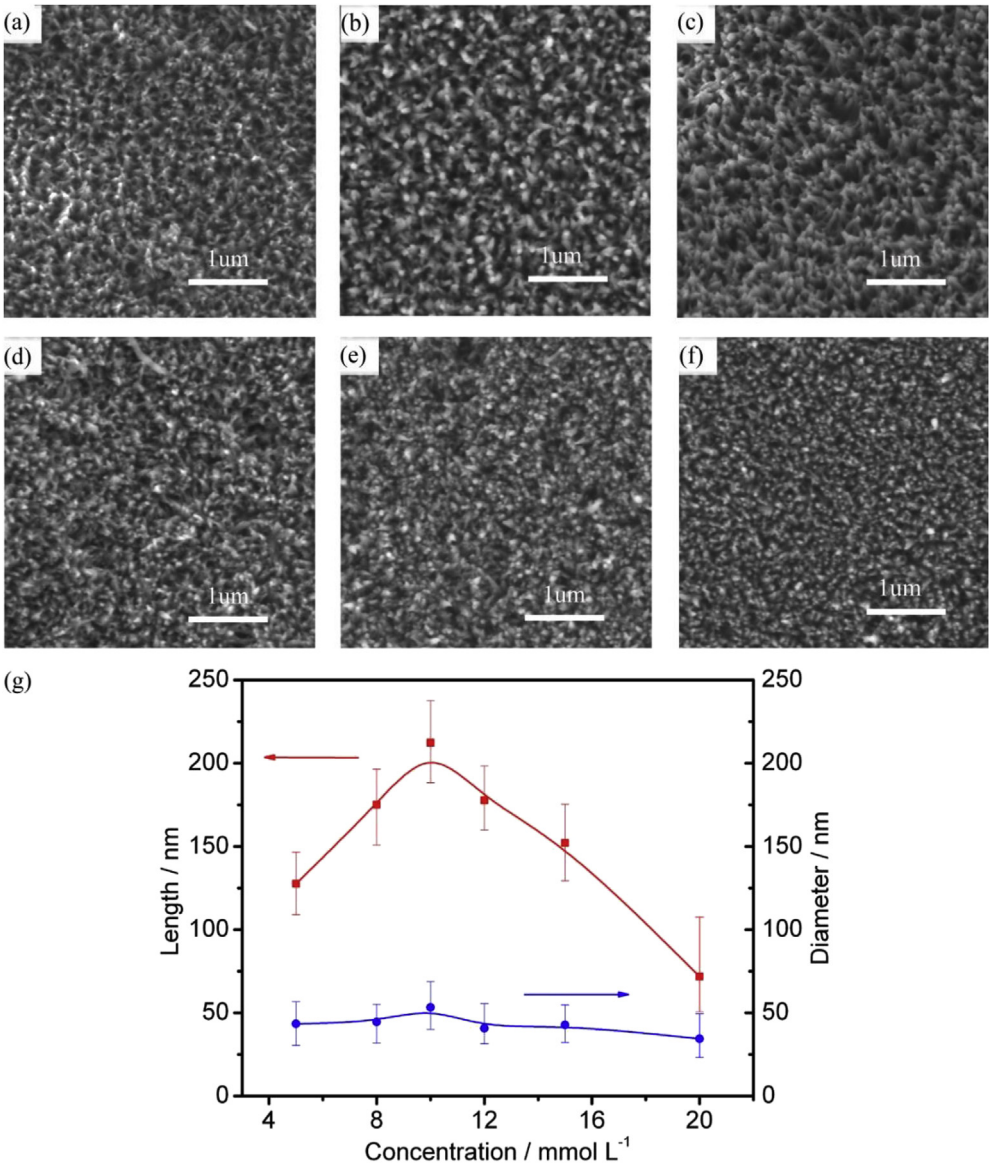

Fig. 4 – SEM images at top view of PANI-C5 (a), PANI-C8 (b), PANI-C10 (c), PANI-C12 (d), PANI-C15 (e) and PANI-C20 (f). The variation of the lengths and the diameters of PANI nanorods polymerized at different concentrations of aniline monomer (g).

work on enhancing the performance of PEMFCs will be carried on.

To research the ordered structure of cathode CL on the influence of PEMFC stability, the long-term durability of the PEMFCs with PANI-C10 and without PANI was examined in a single cell using accelerated stress tests (ASTs) [32]. As shown in Fig. 7, the polarization curves for the PEMFC with PANI-C10 exhibit a mitigated degradation rate compared with the PEMFC without PANI as the potential cycling number increased. The current density at 0.5 V for the PEMFC with PANI-C10 degrades by 42.9% after 5000 cycles (Fig. 7a), whereas a remarkable loss of 69.2% for the PEMFC without PANI is observed (Fig. 7b).

To understand the causes for the performance differences of PEMFCs with and without PANI nanorods, oxygen gain and EIS were carried out. Often, a pair of H_2/O_2 and H_2/air performance curves at the same total pressure is used to determine mass transfer limitations. The difference in cell voltage between the pair of curves is referred to as the "oxygen gain" [33]. High oxygen gain is an indication of high mass transfer loss in the electrode at the same current density [34]. The PEMFCs with PANI nanorods show lower oxygen gain than PEMFC without PANI (Fig. 8a), indicating that the PANI nanorods can facilitate the oxygen transport. The PEMFC with PANI-C10 shows the lowest oxygen gain. Consequently, the PEMFC with PANI-C10 exhibits the best performance. Mass transport effect appears at high current density can be evaluated by EIS. The EIS and the electrical equivalent circuit are shown in Fig. 8b [35,36]. The arc appeared at the higher frequency is due to the charge transfer impedance and the double layer capacitance, and the low frequency arc is caused by the mass transport impedance [37]. However, when the

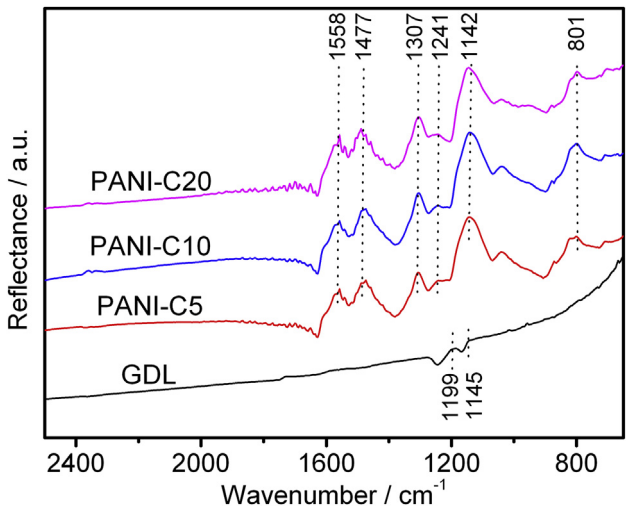

Fig. 5 – ATR-FTIR spectra of the GDL, PANI-C5, PANI-C10 and PANI-C20.

Table 1 – Property of PANI nanorods.

Sample	PANI-C5	PANI-C10	PANI-C20
Conductivity (S cm^{-1})	3.93 ± 0.11	10.31 ± 0.58	4.07 ± 0.09
Density (μm^{-2})	63 ± 5	37 ± 3	143 ± 6
Porosity (%)	90.65 ± 0.74	91.75 ± 0.67	86.72 ± 0.56

time constants for the kinetic and mass transfer process are not sufficiently different, the total arc reflects the over-lapping of the two arcs [2,38]. The electrochemical parameters determined from the EIS data are listed in Table 2. The charge transfer resistances of the four PEMFCs are similar, which is agree with the identical loading of Pt in the cathode. The mass transfer resistance of the PEMFC without PANI is 0.270 Ω cm^2, which is larger than that of the PEMFCs with PANI nanorods. So the oxygen transport resistance of the PEMFC without PANI is higher than that of PEMFCs with PANI nanorods at 1000 mA cm^{-2}. The mass transfer resistances of the PEMFCs with PANI nanorods have negative correlation with the porosities of the PANI nanorods layers. The mass transfer resistances of the PEMFCs decrease in the order PANI-C20 (0.244 Ω cm^2)>PANI-C5 (0.239 Ω cm^2)>PANI-C10 (0.180 Ω cm^2). The opposite order of porosity is observed for these samples in Table 1; that is, PANI-C10 (91.75%)>PANI-C5 (90.65%)>PANI-C20 (86.72%). So the high porosity is benefit for the oxygen transport.

The oxygen gain and EIS show that the oxygen transport resistances of the CLs with the PANI nanorods are lower than that of CL without PANI. Because the aligned PANI nanorods enhance the porosity and reduce the tortuosity of the CL, bringing about low oxygen transport resistance, which is helpful to reduce the mass transfer polarization and enhance the performance of PEMFCs.

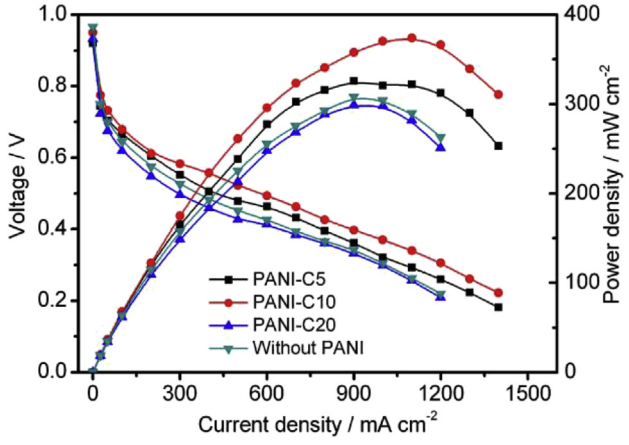

Fig. 6 – Polarization curves and power density curves of the PEMFCs with PANI-C5, PANI-C10, PANI-C20 and without PANI, operated at 80 °C with H_2 and O_2 flow rates of 200 and 400 mL min^{-1}, respectively.

Conclusions

In summary, aligned PANI nanorods are in situ synthesized on the porous GDL. The length and diameter of PANI nanorods

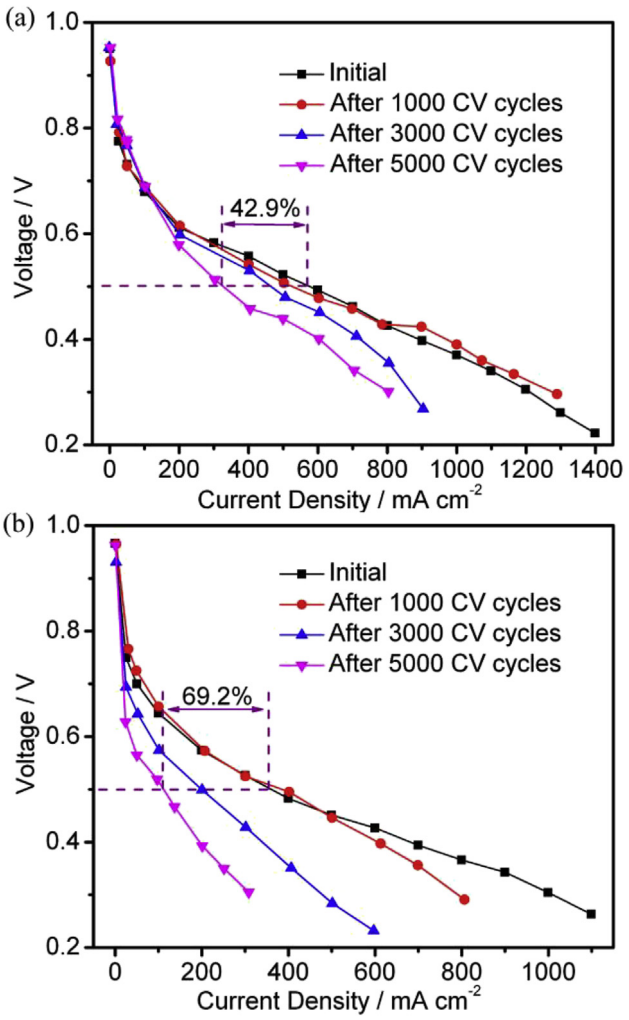

Fig. 7 – Polarization curves after different ASTs cycles for PEMFCs with PANI-C10 (a) and without PANI (b).

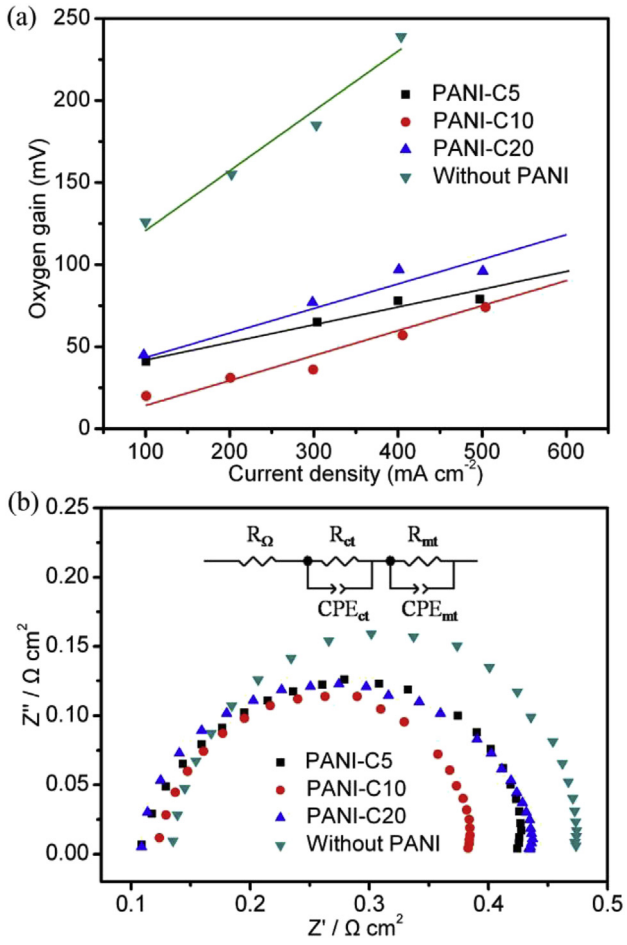

Fig. 8 – Oxygen gain (a) and EIS at 1000 mA cm^{-2} (b) of the PEMFCs with PANI-C5, PANI-C10, PANI-C20 and without PANI. (R_Ω: ohmic resistance; R_{ct}: charge transfer resistance; R_{mt}: mass transport resistance; CPE_{ct} and CPE_{mt}: constant phase elements connected in parallel with charge transfer and mass transport resistances.)

can be facilely controlled via altering the concentration of aniline monomer or the reaction temperature during the in situ polymerization process. The longest PANI nanorods are obtained when the concentration of aniline monomer is 10 mmol L^{-1} and the temperature is 0 °C, which may be ascribed to the proper rate of polymerization. The PEMFC with the PANI-C10 sample gets the highest performance with a mass specific power density of 2.5 kW g_{Pt}^{-1} (as the cathode), which is 21% higher than that of the PEMFC without PANI nanorods. This improvement can be attributed to the reduced oxygen transport resistance, which is proved combining oxygen gain and EIS. This study provides a facile method to prepare spatially ordered CLs of fuel cells in a large scale.

Table 2 – Electrochemical parameters determined from the EIS data.

PEMFCs	R_Ω(Ω cm^2)	R_{ct}(Ω cm^2)	R_{mt}(Ω cm^2)
PANI-C5	0.107	0.091	0.239
PANI-C10	0.125	0.090	0.180
PANI-C20	0.100	0.091	0.244
Without PANI	0.125	0.090	0.270

Acknowledgments

The authors appreciate the financial supports of the National Basic Research Program of China (2012CB215500), the High Technology Research and Development Program of China (2012AA053401), the "Strategic Priority Research Program" of the Chinese Academy of Sciences (XDA09030104) and the National Natural Science Foundation of China (21406222).

REFERENCES

[1] Xie Z, Tang X, Yang P, Sun M, Yang K, Huang Q. Carboxyl-terminated butadiene-acrylonitrile-modified carbon paper for use of gas diffusion layer in PEM fuel cells. Int J Hydrogen Energy 2015;40:14345–52.
[2] Mason TJ, Millichamp J, Shearing PR, Brett DJL. A study of the effect of compression on the performance of polymer electrolyte fuel cells using electrochemical impedance spectroscopy and dimensional change analysis. Int J Hydrogen Energy 2013;38:7414–22.
[3] Zenyuk IV, Medici E, Allen J, Weber AZ. Coupling continuum and pore-network models for polymer-electrolyte fuel cells. Int J Hydrogen Energy 2015;40:16831–45.
[4] Döner A, Solmaz R, Kardaş G. Fabrication and characterization of alkaline leached CuZn/Cu electrode as anode material for direct methanol fuel cell. Energy 2015;90(Part 1):1144–51.
[5] Choo M-J, Oh K-H, Kim H-T. Analysis of oxygen transport in cathode catalyst layer of low-Pt-loaded fuel cells. Chem Electro Chem 2015;2:382–8.
[6] Yuan T, Zou Z, Chen M, Li Z, Xia B, Yang H. New anodic diffusive layer for passive micro-direct methanol fuel cell. J Power Sources 2009;192:423–8.
[7] Wu H, Yuan T, Huang Q, Zhang H, Zou Z, Zheng J, et al. Polypyrrole nanowire networks as anodic micro-porous layer for passive direct methanol fuel cells. Electrochim Acta 2014;141:1–5.
[8] Middelman E. Improved PEM fuel cell electrodes by controlled self-assembly. Fuel Cells Bull 2002;2002:9–12.
[9] Ahluwalia RK, Wang X, Lajunen A, Steinbach AJ, Hendricks SM, Kurkowski MJ, et al. Kinetics of oxygen reduction reaction on nanostructured thin-film platinum alloy catalyst. J Power Sources 2012;215:77–88.
[10] Rabat H, Andreazza C, Brault P, Caillard A, Béguin F, Charles C, et al. Carbon/platinum nanotextured films produced by plasma sputtering. Carbon 2009;47:209–14.
[11] Melechko AV, Merkulov VI, McKnight TE, Guillorn MA, Klein KL, Lowndes DH, et al. Vertically aligned carbon nanofibers and related structures: controlled synthesis and directed assembly. J Appl Phys 2005;97:041301.
[12] Tian ZQ, Lim SH, Poh CK, Tang Z, Xia Z, Luo Z, et al. A highly order-structured membrane electrode assembly with vertically aligned carbon nanotubes for ultra-low Pt loading PEM fuel cells. Adv Energy Mater 2011;1:1205–14.
[13] Bonakdarpour A, Tucker RT, Fleischauer MD, Beckers NA, Brett MJ, Wilkinson DP. Nanopillar niobium oxides as support structures for oxygen reduction electrocatalysts. Electrochim Acta 2012;85:492–500.

[14] Christwardana M, Kwon Y. Effects of multiple polyaniline layers immobilized on carbon nanotube and glutaraldehyde on performance and stability of biofuel cell. J Power Sources 2015;299:604–10.
[15] Zhiani M, Gharibi H, Kakaei K. Optimization of Nafion content in Nafion–polyaniline nano-composite modified cathodes for PEMFC application. Int J Hydrogen Energy 2010;35:9261–8.
[16] Jin J, Wang Q, Haque MA. Length-scale effects on electrical and thermal transport in polyaniline thin films. Org Electron 2010;11:29–35.
[17] Sadeghifar H, Bahrami M, Djilali N. A statistically-based thermal conductivity model for fuel cell gas diffusion layers. J Power Sources 2013;233:369–79.
[18] Liang L, Liu J, Windisch CF, Exarhos GJ, Lin YH. Direct assembly of large arrays of oriented conducting polymer nanowires. Angew Chem Int Ed 2002;41:3665–8.
[19] Chiou N-R, Lui C, Guan J, Lee LJ, Epstein AJ. Growth and alignment of polyaniline nanofibres with superhydrophobic, superhydrophilic and other properties. Nat Nanotech 2007;2:354–7.
[20] Xu J, Wang K, Zu S-Z, Han B-H, Wei Z. Hierarchical nanocomposites of polyaniline nanowire arrays on graphene oxide sheets with synergistic effect for energy storage. Acs Nano 2010;4:5019–26.
[21] Chiou NR, Epstein AJ. Polyaniline nanofibers prepared by dilute polymerization. Adv Mater 2005;17:1679–83.
[22] Jing M, Jiang L, Wang S, Jing F, Sun G. Application of FTIR in direct methanol fuel cells – quantitative analysis of PTFE in gas diffusion layers. Int J Hydrogen Energy 2013;38:7957–63.
[23] Pan LJ, Pu L, Shi Y, Song SY, Xu Z, Zhang R, et al. Synthesis of polyaniline nanotubes with a reactive template of manganese oxide. Adv Mater 2007;19:461–4.
[24] Sapurina I, Mokeev M, Lavrentev V, Zgonnik V, Trchová M, Hlavatá Dr, et al. Polyaniline complex with fullerene C60. Eur Polym J 2000;36:2321–6.
[25] Wu G, Johnston CM, Mack NH, Artyushkova K, Ferrandon M, Nelson M, et al. Synthesis–structure–performance correlation for polyaniline–Me–C non-precious metal cathode catalysts for oxygen reduction in fuel cells. J Mater Chem 2011;21:11392–405.
[26] Torkavannejad A, Sadeghifar H, Pourmahmoud N, Ramin F. Novel architectures of polymer electrolyte membrane fuel cells: efficiency enhancement and cost reduction. Int J Hydrogen Energy 2015;40:12466–77.
[27] Sadeghifar H, Djilali N, Bahrami M. A compact closed-form Nusselt formula for laminar longitudinal flow between rectangular/square arrays of parallel cylinders with unequal row temperatures. Int J Therm Sci 2016;100:248–54.
[28] Sadeghifar H, Djilali N, Bahrami M. Thermal conductivity of a graphite bipolar plate (BPP) and its thermal contact resistance with fuel cell gas diffusion layers: effect of compression, PTFE, micro porous layer (MPL), BPP out-of-flatness and cyclic load. J Power Sources 2015;273:96–104.
[29] Sadeghifar H, Djilali N, Bahrami M. A new model for thermal contact resistance between fuel cell gas diffusion layers and bipolar plates. J Power Sources 2014;266:51–9.
[30] Sadeghifar H, Djilali N, Bahrami M. Effect of polytetrafluoroethylene (PTFE) and micro porous layer (MPL) on thermal conductivity of fuel cell gas diffusion layers: modeling and experiments. J Power Sources 2014;248:632–41.
[31] Wang Y-J, Wilkinson DP, Zhang J. Noncarbon support materials for polymer electrolyte membrane fuel cell electrocatalyst. Chem Rev 2011;111:7625–51.
[32] Xia Z, Wang S, Jiang L, Sun H, Liu S, Fu X, et al. Bio-inspired construction of advanced fuel cell cathode with Pt anchored in ordered hybrid polymer matrix. Sci Rep 2015;5:16100.
[33] Kocha SS. Principles of MEA preparation. Handbook of fuel cells. John Wiley & Sons, Ltd; 2010.
[34] Xia Z, Wang S, Jiang L, Sun H, Sun G. Controllable synthesis of vertically aligned polypyrrole nanowires as advanced electrode support for fuel cells. J Power Sources 2014;256:125–32.
[35] Asghari S, Mokmeli A, Samavati M. Study of PEM fuel cell performance by electrochemical impedance spectroscopy. Int J Hydrogen Energy 2010;35:9283–90.
[36] Solmaz R. Electrochemical preparation and characterization of C/Ni–NiIr composite electrodes as novel cathode materials for alkaline water electrolysis. Int J Hydrogen Energy 2013;38:2251–6.
[37] Su K, Sui S, Yao X, Wei Z, Zhang J, Du S. Controlling Pt loading and carbon matrix thickness for a high performance Pt-nanowire catalyst layer in PEMFCs. Int J Hydrogen Energy 2014;39:3397–403.
[38] Xie Z, Chen G, Yu X, Hou M, Shao Z, Hong S, et al. Carbon nanotubes grown in situ on carbon paper as a microporous layer for proton exchange membrane fuel cells. Int J Hydrogen Energy 2015;40:8958–65.